JACS
JOURNAL OF THE AMERICAN CHEMICAL SOCIETY
Article
pubs.acs.org/JACS

Proton-Coupled Electron Transfer Cleavage of Heavy-Atom Bonds in Electrocatalytic Processes. Cleavage of a C−O Bond in the Catalyzed Electrochemical Reduction of CO_2

Cyrille Costentin,* Samuel Drouet, Guillaume Passard, Marc Robert, and Jean-Michel Savéant*

Université Paris Diderot, Sorbonne Paris Cité, Laboratoire d'Electrochimie Moléculaire, Unité Mixte de Recherche Université - CNRS No 7591, Bâtiment Lavoisier, 15 rue Jean de Baïf, 75205 Paris Cedex 13, France

Supporting Information

ABSTRACT: Most of the electrocatalytic processes of interest in the resolution of modern energy challenges are associated with proton transfer. In the cases where heavy atom bond cleavage occurs concomitantly, the question arises of the exact nature of its coupling with proton−electron transfer within the catalytic cycle. The cleavage of a C−O bond in the catalyzed electrochemical conversion of CO_2 to CO offers the opportunity to address this question. Electrochemically generated iron(0) porphyrins are efficient, specific, and durable catalysts provided they are coupled with Lewis or Brönsted acids. The cocatalyst properties of four Brönsted acids of increasing strength, water, trifluoroethanol, phenol, and acetic acid, have been systematically investigated. Preparative-scale electrolyses showed that carbon monoxide is the only product of the catalytic reaction. Methodic application of a nondestructive technique, cyclic voltammetry, with catalyst and CO_2 concentrations, as well as H/D isotope effect, as diagnostic parameters allowed the dissection of the reaction mechanism. It appears that the key step of the reaction sequence consists of an electron transfer from the catalyst concerted with the cleavage of a C−O bond and the transfer of one proton. This is the second example, and an intermolecular version of such a concerted proton−electron bond-breaking reaction after a similar electrochemical process involving the cleavage of O−O bonds has been identified. It is the first time that a proton−electron transfer concerted with bond breaking has been uncovered as the crucial step in a catalytic multistep reaction.

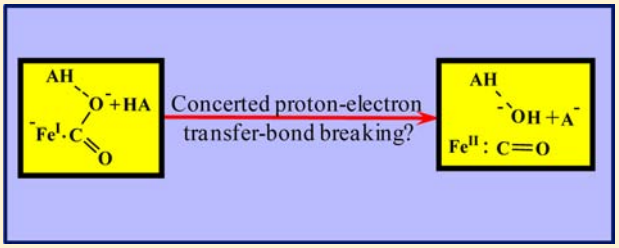

INTRODUCTION

That proton transfers are implicated in most cases in the activation of small molecules, particularly those implicated in the resolution of modern energy challenges, appears if only on thermodynamical grounds as exemplified in Figure 1. The catalytic transformation of carbon dioxide to fuels is one of the most important contemporary energy and environmental issues. CO_2 is a very inert molecule toward reduction.[1] Its conversion into liquid fuels therefore raises formidable challenges in terms of energy and activation. Focusing on the "easiest" conversion, i.e., conversion to carbon monoxide, a number of catalysts, mostly low oxidation states of transition metal complexes, have been proposed.[2−12] Among them, iron(0) porphyrins, electrochemically generated at a mercury or a glassy carbon electrode, are efficient, specific, and durable catalysts provided they are coupled with Lewis acids or weak Brönsted acids.[13,14] In the latter case, the added acids were selected as being weak to avoid proton reduction leading to hydrogen evolution as previously noted with the same catalyst when using Et_3NH^+ as an acid.[15] The strongest acid investigated was trifluoroethanol (TFE), used only in a large concentration range (0.25−4 M).

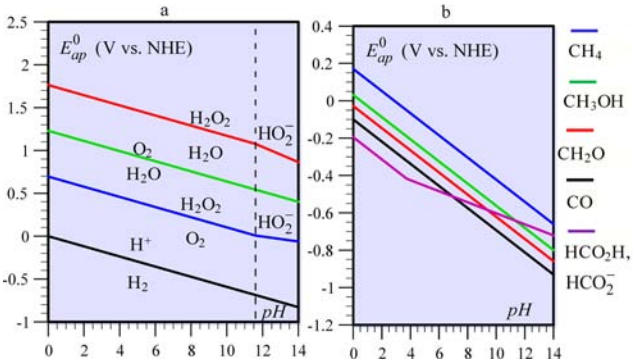

Figure 1. Pourbaix diagrams for the oxidation of water and reduction of dioxygen (a) and reduction of carbon dioxide (b).

We have found that catalysis of the conversion of CO_2 to CO by electrogenerated iron(0) porphyrins can also be obtained with stronger acids such as phenol (PhOH) and acetic acid (AcOH). The effect of a weaker acid, trifluoroethanol, was systematically re-examined in concentration ranges more varied than previously performed.[13b] The role of water as proton donor was also examined, per se, because some water is inevitably present in small but non-negligible quantities that could possibly influence the effect of the other acids. The cyclic voltammetric responses show

Received: March 25, 2013
Published: May 21, 2013

   dx.doi.org/10.1021/ja4030148 | J. Am. Chem. Soc. 2013, 135, 9023−9031

considerable acceleration of catalysis by addition of acids. However, it soon appeared that the canonical S-shape wave expected for fast catalytic reactions is not observed in a number of cases, particularly when catalysis is strong. This behavior is caused by side-phenomena whose contributions are all the more important when the catalytic current is high.[16] We consequently resort to the recently proposed "foot-of-the-wave" (FOW) strategy[16] to circumvent these difficulties. The present work is not a continued methodological contribution aiming at a further validation of the FOW method. Instead, the FOW methodology, the validity of which has been previously established,[16] is systematically applied to the rigorous determination of the reactions order on which the mechanism analysis is based. These results allowed us to gain new insights into the mechanism according to which proton transfer is associated to the key step of the CO_2 to CO conversion, namely the cleavage of a carbon−oxygen bond. Since the first reports on the catalysis of CO_2 reduction by iron(0) porphyrins, proton-coupled electron transfers (PCET) have received a lot of attention, with particular emphasis on concerted (CPET) pathways.[17−22] Of special relevance to the present discussion is the recent finding that O−O bonds can be broken by proton and electron transfer along an all-concerted pathway. A general kinetic model of processes in which a heavy-atom bond is broken concertedly with a concerted proton−electron transfer was established on this occasion.[23]

The paper is organized as follows. The cyclic voltammetric responses are first reported in a qualitative manner, showing the huge acceleration of catalysis by addition of acids. The results of the preparative-scale electrolyses are then described, confirming the formation of CO as the major product that was already observed in the cyclic voltammograms. They allow estimation of the faradaic yield and turnover frequency and of the time-decay of the catalyst. These observations served as a starting point for a quantitative FOW analysis of the cyclic voltammetric responses, recorded as a function of the acid concentration as the main operational parameter. One of the important outcomes of this detailed kinetic analysis is that it points to the occurrence of an electron transfer concerted with the C−O bond cleavage and with the transfer of one proton.

RESULTS AND DISCUSSION

1. Raw Cyclic Voltammetric Data. Qualitative Trends. Figure 2 shows a typical example of the catalytic reduction of CO_2 by Fe^0TPP (TPP: tetraphenylporphyrin) in the presence of an acid, AH. Starting with Fe^{II}TPP, two reversible reduction waves are observed in the absence of CO_2 and AH corresponding successively to the generation of Fe^{I}TPP and Fe^{0}TPP. Addition of CO_2 and AH does not change the first wave but produces a drastic increase and change in shape of the second wave. The second wave is almost independent of the scan rate. It is the result of the catalytic reaction[24] sketched in the upper insert of Figure 2.

That carbon monoxide is the main product of such catalytic reductions of CO_2 will be fully demonstrated from preparative-scale electrolyses later on. Note that the presence of CO is apparent in the backward trace of the catalytic current. It is indeed well-known that iron(II) porphyrins strongly bind CO. The small wave around −1.0 V thus corresponds to the oxidation of Fe^{I}TPP into the strongly stabilized O═C:Fe^{II}TPP complex, resulting in a substantial shift of the Fe^{I}TPP oxidation potential (see lower insert in Figure 2).

2. Preparative Scale Electrolyses. The electrolyses (see Experimental Section) were carried out in *N*,*N*′-dimethylformamide (DMF) in the presence of 0.1 M *n*-Bu_4NPF_6 at a mercury pool working electrode, with [FeTPP] = 1 mM, the solution being saturated with CO_2 (0.23 M) and with various concentrations of CF_3CH_2OH, PhOH, and AcOH (Table 1). The electrolysis potential was −1.46 V vs NHE. The gas phase was analyzed by gas chromatography and the liquid phase by ionic chromatography. After 1 h electrolysis, no formate, no oxalate, and practically no hydrogen were detected with all three acids. The only product was CO in all cases. With PhOH and CF_3CH_2OH, the CO faradaic yield was close to quantitative (Table 1). With AcOH, the CO faradaic yield was only 31% and, after 40 min, the solution took the green color of successive $2H^+ + 2e^-$ reduction products such as the TPP analogues of chlorin, bateriochlorin,[25] and further hydrogenation products of the porphyrin ring. Although their precise identification is beyond the scope of the present work, these reactions may be held responsible for the low CO faradaic yield in this case (a $8H^+ + 8e^-$ hydrogenation of the porphyrin ring corresponds to a 62% faradaic yield).

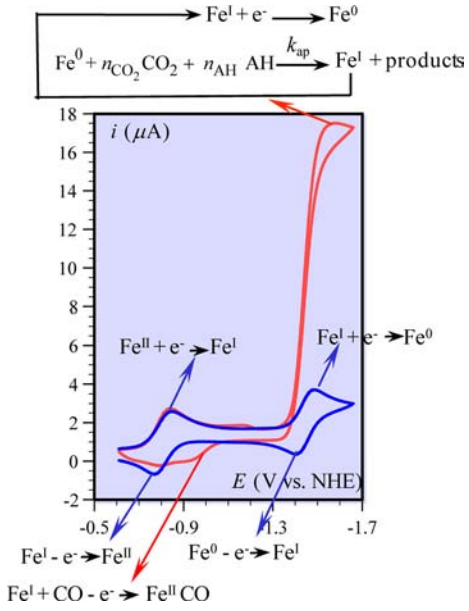

Figure 2. Cyclic voltammetry of FeTPP (1 mM) in DMF + 0.1 M *n*-Bu_4NPF_6, in the absence (blue) and presence of 0.23 M CO_2 and of 10 mM PhOH (red). Sketch of the electrochemical reactions.

Table 1. Preparative-Scale Electrolyses

acid	concentration (M)	faradaic yield (%)
CF_3CH_2OH	0.1	97
	0.5	98
	1	100
PhOH	0.1	100
	0.5	98
	1	94
AcOH	0.1	31

3. Foot-of-the-Wave Analysis of the Cyclic Voltammetric Responses. Typical cyclic voltammetric catalytic responses are shown in Figure 3 for PhOH and AcOH and in Figure 4 for CF_3CH_2OH and water. More are available in the Supporting Information concerning PhOH and CF_3CH_2OH for other values of the H_2O concentration.

A first remark is that addition of these acids may result in a considerable increase in the catalytic current, reaching values as high as 100 electrons per molecule. Simultaneously, the current−potential

dx.doi.org/10.1021/ja4030148 | J. Am. Chem. Soc. 2013, 135, 9023−9031

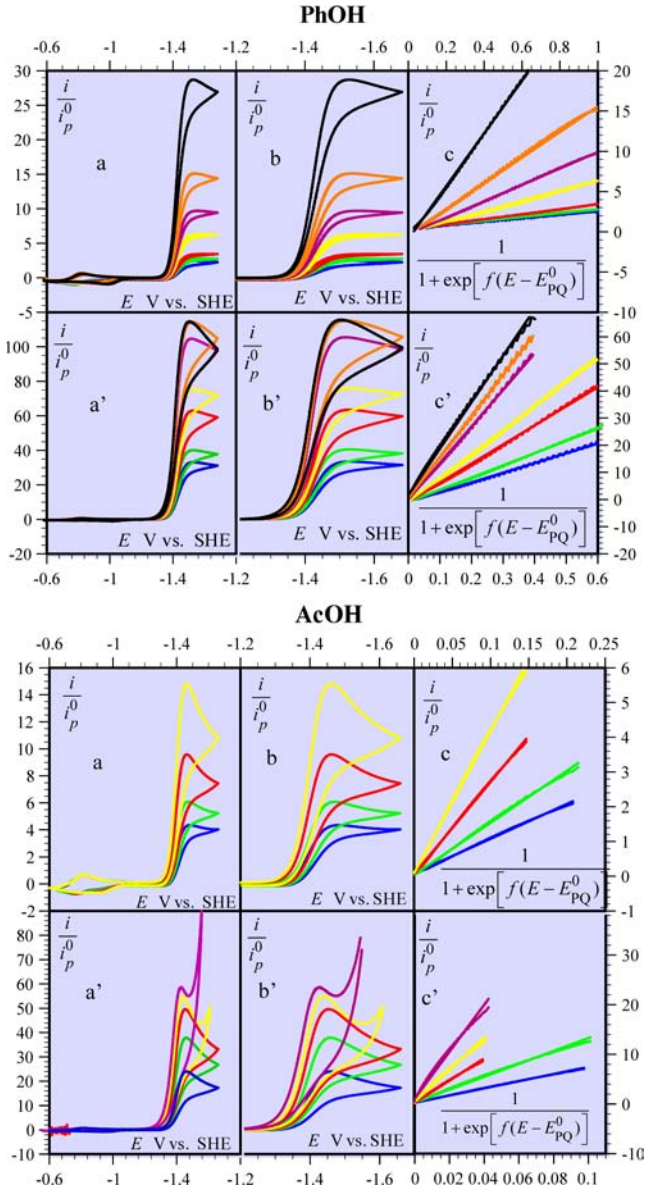

Figure 3. Cyclic voltammetry (0.1 V s^{-1}) and FOW analysis of the catalysis of CO_2 reduction by Fe(0)TPP as a function of acid addition. FeTPP (1 mM) in DMF + 0.1 M *n*-Bu_4NPF_6, in the presence of 0.23 M CO_2. a, a′: cyclic voltammogram starting with Fe(II)TPP. b, b′: Fe(I/0) catalytic wave. c, c′: FOW analysis of the catalytic wave ($E^0_{PQ} = -1.428$ V vs SHE). PhOH (+ 20 mM H_2O): a, b, c: from bottom to top: [PhOH] (mM): 0, 1, 2, 5, 10, 20, 50. a′, b′, c′: from bottom to top: [PhOH] (mM): 100, 200, 500, 1000, 2000, 3000, 4000. AcOH: a, b, c: from bottom to top: [AcOH] (mM): 1, 2, 5, 10. a′, b′, c′: from bottom to top: [AcOH] (mM): 20, 50, 100, 200, 500.

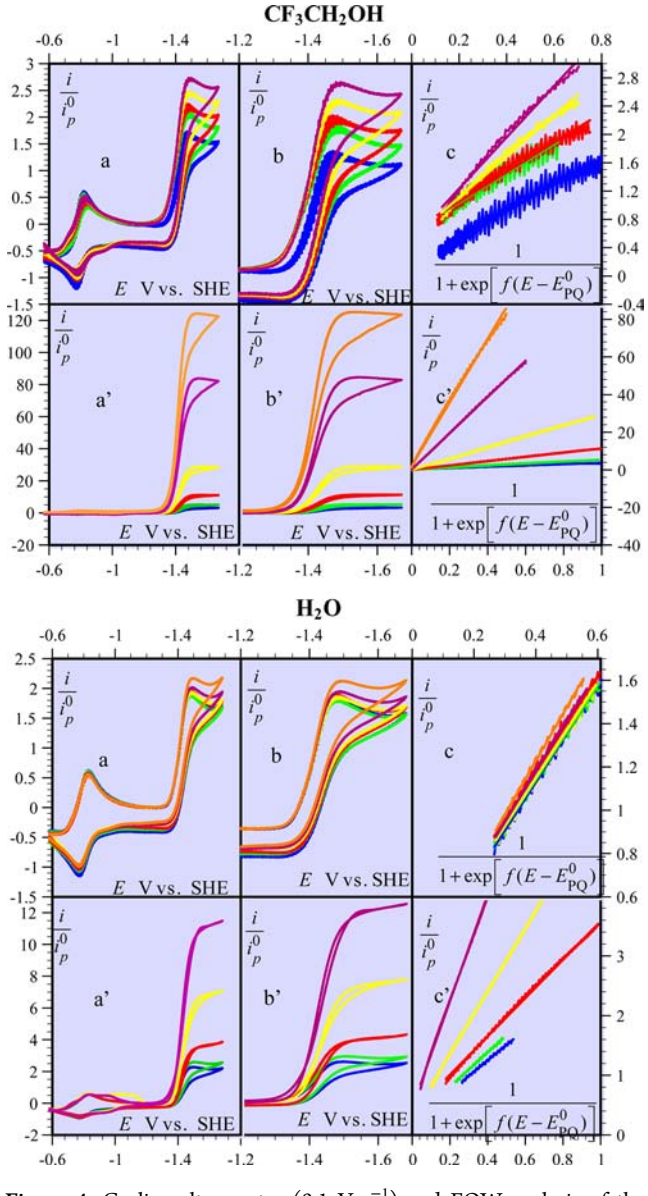

Figure 4. Cyclic voltammetry (0.1 V s^{-1}) and FOW analysis of the catalysis of CO_2 reduction by Fe(0)TPP as a function of acid addition. FeTPP (1 mM) in DMF + 0.1 M *n*-Bu_4NPF_6, in the presence of 0.23 M CO_2. a, a′: cyclic voltammogram starting with Fe(II)TPP. b, b′: Fe(I/0) catalytic wave. c, c′: FOW analysis of the catalytic wave ($E^0_{PQ} = -1.428$ V vs SHE). CF_3CH_2OH (+ 20 mM H_2O): a, b, c: from bottom to top: [CF_3CH_2OH] (mM): 0, 1, 2, 5, 10. a′, b′, c′: from bottom to top: [CF_3CH_2OH] (mM): 20, 50, 100, 200, 500, 1000. H_2O: a, b, c: from bottom to top: [H_2O] (mM): 0, 1, 2, 5, 10, 20. a′, b′, c′: from bottom to top: [H_2O] (mM): 50, 100, 200, 500, 1000.

responses are far from the canonical S-shape curves, the more so the higher the catalytic current. This led us to apply the FOW strategy as depicted in Figures 3 and 4. In doing so, the catalytic current−potential curve was corrected by subtraction of the current of the Fe(II)/Fe(I) wave at the foot of the catalytic wave. This correction is approximate because it does not take into account the diffusion tailing of the Fe(II)/Fe(I) wave in the potential range of the catalytic wave. The resulting error is however negligible in most cases. In Figures 3 and 4, the current has been normalized toward the peak current of the one-electron Fe(II)/Fe(I) reversible wave, i_p^0, leading to application of the following equation to the FOW analysis:

$$\frac{i}{i_p^0} = \frac{2.24\sqrt{\frac{RT}{Fv}2k_{obs}}}{1+\exp\left[\frac{F}{RT}(E-E^0_{PQ})\right]} = \frac{2.24\sqrt{\frac{RT}{Fv}2k_{ap}[CO_2]}}{1+\exp\left[\frac{F}{RT}(E-E^0_{PQ})\right]}$$

E^0_{PQ} is the standard potential of the Fe^I/Fe^0 catalyst couple, in agreement with the observation that the reaction order with respect to CO_2 is 1 (section 3.5). The ensuing variations in the global catalytic rate constant, k_{ap}, with the concentration of acids are summarized in Figure 5. They suggest the reaction mechanism depicted in Scheme 1 as justified by following detailed analysis in the case of each acid. The validity of Scheme 1 requires

dx.doi.org/10.1021/ja4030148 | J. Am. Chem. Soc. 2013, 135, 9023−9031

that CO is the sole reaction product. This is unambiguously the case with PhOH and CF_3CH_2OH as seen in section 2. With AcOH this is also the case at the foot of the wave, where the effect of catalyst deactivation is minimized, as attested by the linearity of the FOW analysis in the range used for deriving the reaction kinetics.[16] Besides the main acids that we have tested, PhOH, CF_3CH_2OH, and AcOH, the role of water, residual water with a concentration $[H_2O]_r$ or added water, $[H_2O]$, as an acid has also been taken into account even though it is expected to give rise to a catalysis weaker than that of the main acids. The same applies to CO_2 itself, acting as a Lewis acid favoring catalysis.[13c] The various contributions to the apparent catalytic rate constant are summarized in eq 1 (see Supporting Information (SI)) within assumptions detailed below:

$$k_{ap} = K_1\left\{k_0[CO_2] + \frac{k'_2[H_2O]_r(k'_0[H_2O]_r + k''_0[CO_2])}{k'_{-2} + k'_3[AH]} + \left[\frac{k_2(k''_3[H_2O]_r + k'''_3[CO_2])}{k_{-2} + k_3[AH]} + \frac{k'_2[H_2O]_r k'_3}{k'_{-2} + k'_3[AH]}\right][AH] + \frac{k_2k_3}{k_{-2} + k_3[AH]}[AH]^2\right\} \quad (1)$$

Equation 1 assumes that addition of CO_2 onto Fe(0) remains at equilibrium. This is justified by the experimental observation that at the highest acid concentration investigated there is not zero order with respect to AH. It also assumes that $k_{-2} \gg k''_3[H_2O]_r + k'''_3[CO_2]$ and $k'_{-2} \gg k'_0[H_2O]_r + k''_0[CO_2]$, meaning that H_2O and CO_2 are too weak as acids to make steps 2 and 2′ irreversible.

3.1. Water. Equation 1, recast for water, involves three terms with reaction orders of added H_2O equal to 0, 1, and 2, respectively:

$$k_{ap} = K_1\left\{k_0[CO_2] + \frac{(k_0[CO_2] + k'_2[H_2O]_r)(k''_0[CO_2] + k'_0[H_2O]_r)}{k'_{-2}}\right\} + K_1\left\{\frac{[k'_0(k_0[CO_2]) + k'_2(k''_0[CO_2])]}{k'_{-2}} + 2K'_2k'_0 \times [H_2O]_r\right\}[H_2O] + K_1K'_2k'_0[H_2O]^2 \quad (2)$$

$K_1\{k_0[CO_2] + ((k_0[CO_2] + k'_2[H_2O]_r)(k''_0[CO_2] + k'_0[H_2O]_r))/(k'_{-2})\} = 8.5\ M^{-1}\ s^{-1}$ is obtained from experiments with no added water. $K_1\{([k'_0(k_0[CO_2]) + k'_2(k''_0[CO_2])/k'_{-2}) + 2K'_2k'_0[H_2O]_r)\} = 50\ M^{-2}\ s^{-1}$ is obtained from the first-order fitting (magenta line) of the low H_2O-concentration data of Figure 5:

$$k_{ap} = K_1\left\{k_0[CO_2] + \frac{(k_0[CO_2] + k'_2[H_2O]_r)(k''_0[CO_2] + k'_0[H_2O]_r)}{k'_{-2}}\right\} + K_1\left\{\frac{[k'_0(k_0[CO_2]) + k'_2(k''_0[CO_2])]}{k'_{-2}} + 2K'_2k'_0[H_2O]_r\right\}[H_2O]$$

$K_1K'_2k'_0 = 100\ M^{-3}\ s^{-1}$ is obtained from the second-order fitting (green line) of the high H_2O-concentration data of Figure 5:

$$k_{ap} = K_1\left\{k_0[CO_2] + \frac{(k_0[CO_2] + k'_2[H_2O]_r)(k''_0[CO_2] + k'_0[H_2O]_r)}{k'_{-2}}\right\} + K_1K'_2k'_0[H_2O]^2$$

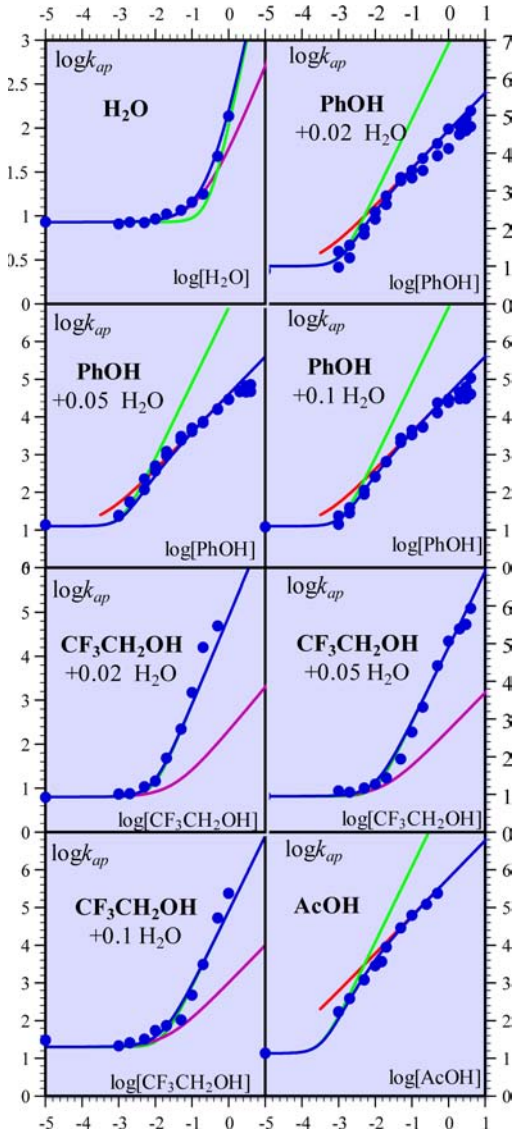

Figure 5. Variations of the apparent catalytic rate constant with the concentration of acids in the presence of variable amounts of water. Concentrations in M, k_{ap} in $M^{-1}\ s^{-1}$. Solid lines: magenta, green, red, and blue: low-concentration first-order, second-order, high-concentration first-order, and global fittings (see text).

The blue line represents the global fitting of the whole set of data points according to eq 2.

3.2. Phenol. Despite their modest contributions, the role of water and CO_2 as acids should be taken into account besides the predominating role of phenol. In the absence of phenol, eq 1 may be written as:

$$k_{ap} = k_i = K_1\{k_0[CO_2] + K'_2[H_2O]_i(k'_0[H_2O]_i + k''_0[CO_2])\} \quad (3)$$

k_i represents the small but non-negligible contribution of water and CO_2 as catalysis boosters.

At low phenol concentrations, $k_{-2} \gg k_3[AH]$ and $k'_{-2} \gg k'_3[AH]$; therefore:

$$k_{ap} = k_i + K_1[K_2(k''_3[H_2O]_i + k'''_3[CO_2]) + K'_2[H_2O]_ik'_3][AH] + K_1K_2k_3[AH]^2$$

dx.doi.org/10.1021/ja4030148 | J. Am. Chem. Soc. 2013, 135, 9023−9031

Scheme 1

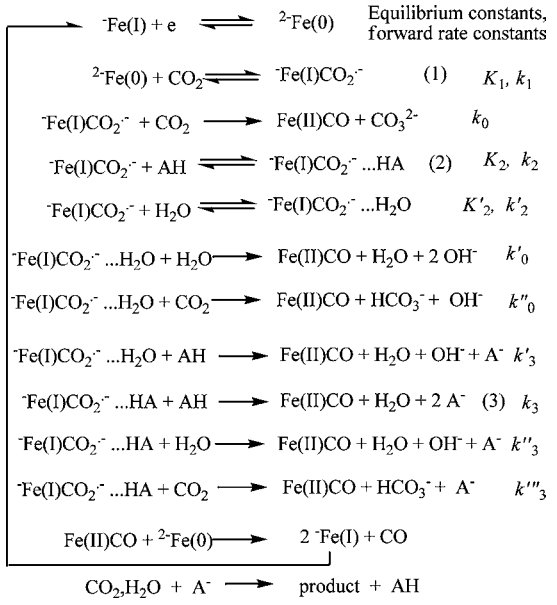

This equation can be simplified to:

$$k_{ap} = k_i + K_1K_2k_3[AH]^2 \quad (4)$$

by noting that no first order is experimentally detected between the zero-order and second-order zones (see Figure 5).

The green line in Figure 5 then represents the fitting of the experimental points obtained at low phenol concentrations by eq 4 with k_i = 8, 8, 11, and 17 M^{-1} s^{-1} at 0 (residual) 0.02, 0.05, and 0.1 M water, respectively, and $K_1K_2k_3 = 8 \times 10^6$ M^{-3} s^{-1}.

At high phenol concentrations, $k_{-2} \ll k_3[AH]$ and $k'_{-2} \ll k'_3[AH]$; therefore:

$$k_{ap} \approx K_1k_2[AH] \quad (5)$$

The straight red line in Figure 5 then represents the fitting of the high phenol concentration points by eq 5, leading to $K_1k_2 = 4 \times 10^4$ M^{-2} s^{-1} (implying that k_3/k_{-2} = 200 M^{-1}).

Finally, the global rate expression for phenol may be simplified as:

$$k_{ap} = k_i + K_1\frac{K_2k_3}{1 + \frac{k_3}{k_{-2}}[AH]}[AH]^2 \quad (6)$$

which has been used to successfully fit the whole set of data points in Figure 5 (blue solid line), thus confirming the preceding parameter values.

3.3. Trifluoroethanol. Unlike the preceding case, it appears that, at small concentrations of CF_3CH_2OH, there is a small but distinct effect from added water, whereas at higher concentrations, the CF_3CH_2OH reaction order is 2 with no effect from added water. Because of the absence of a reaction order of 1 at high acid concentration, $k_{-2}/k_3 > 3$ M. Because of the slight but distinct appearance of a reaction order of 1 at small acid concentrations, $[AH] \ll k_{-2}'/k_3'$. Equation 1 may therefore be simplified to:

$$k_{ap} = k_i + K_1[K_2(k''_3[H_2O]_i + k'''_3[CO_2]) + K'_2k'_3[H_2O]_i] \times [AH] + K_1K_2k_3[AH]^2 \quad (7)$$

where k_i is here, too, defined by eq 3.

The differences in the case of phenol are that (i) the zone where the low-concentration reaction order is 1 cannot be neglected, and that (ii) the zone where the high-concentration reaction order is 1 is not reached within the available range of CF_3CH_2OH concentrations. The data points could then be fitted with a low-concentration reaction order of 1 (magenta line) according to:

$$k_{ap} = k_i + K_1[K_2(k''_3[H_2O]_i + k'''_3[CO_2]) + K'_2k'_3[H_2O]_i][AH]$$

with a reaction order of 2 (green line) according to:

$$k_{ap} = k_i + K_1K_2k_3[AH]^2$$

and with the full eq 7 (blue line in Figure 5).

In all cases k_i has the same values as in the case of phenol. The following values are obtained:

$$K_1[K_2(k''_3[H_2O]_i + k'''_3[CO_2]) + K'_2k'_3[H_2O]_i] \approx 5 \times 10^4\ M^{-3}\ s^{-1}$$

where $K_1K_2k_3 = 8 \times 10^4$ M^{-3} s^{-1}.

3.4. Acetic Acid. As with phenol, there is no zone where the low-concentration reaction order is 1. Instead there is a zone where the reaction order is 2 and a zone where the high-concentration reaction order is 1, leading to the applicability of eq 6 in this case, too. We may thus fit the data in Figure 5 with a reaction order of 2 (green line), of 1 (red line), and with full eq 6 (blue line) leading to:

$$K_1K_2k_3 = 1.2 \times 10^8\ M^{-3}\ s^{-1}$$

where $K_1k_2 = 6 \times 10^5$ M^{-2} s^{-1} (implying that k_3/k_{-2} = 200 M^{-1}).

3.5. Reaction Order with Respect to CO_2. The variation of the cyclic voltammetric responses with the concentration of CO_2 and the ensuing FOW analyses are shown in Figure 6, taking as an example the case of a 0.5 M concentration of added phenol. The linearity of the variation of the pseudo-first-order k_{obs} with CO_2 concentration (Figure 6d) shows that the reaction order with respect to CO_2 is indeed that as implied by Scheme 1.

4. Mechanism. Concerted Proton Electron Transfer and Breaking of One C–O Bond of CO_2. The lengthy reaction sequence in Scheme 1 was necessary to account for the possible role, even though minor, of water and CO_2 itself in the coupling of proton transfer with electron transfer and bond breaking. Taking now each of the four acids individually, the simplified Scheme 2 suffices to compare them provided that specific acid concentration ranges are analyzed (Figure 5 and Table 2).

Focusing now on the mechanism of reaction 3, the addition of the second molecule of AH involves the formation of a precursor complex in which an H-bond is formed between one of the oxygen of CO_2 and this second AH molecule. This adduct may take the two forms depicted at the top of Scheme 3, which correspond each to the following mesomeric forms of the initially formed CO_2 adduct, respectively:

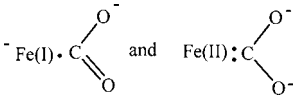

The two possible forms of the precursor complex are correspondingly asymmetrical and symmetrical. The two carbon–oxygen bonds do not play a symmetrical role in the reaction because one bond is broken during the proton-coupled

dx.doi.org/10.1021/ja4030148 | J. Am. Chem. Soc. 2013, 135, 9023–9031

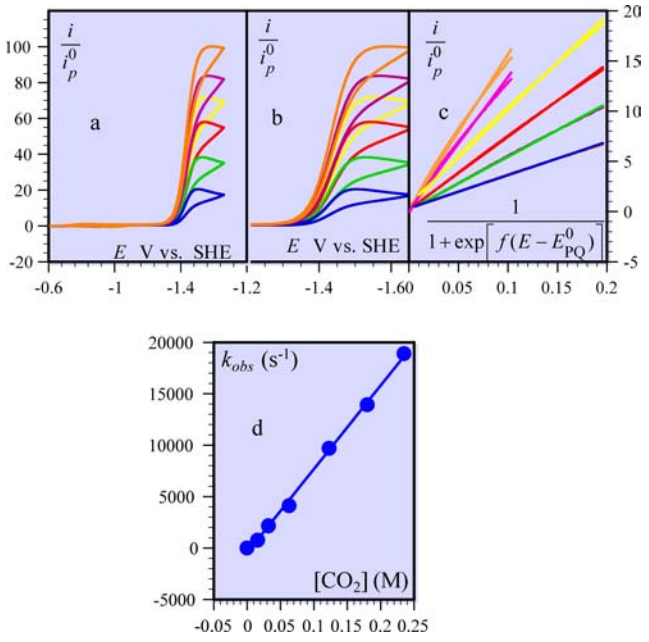

Figure 6. Cyclic voltammetry (0.1 V s^{-1}) and FOW analysis of the catalysis of CO_2 reduction by Fe(0)TPP as a function of CO_2 concentration in the presence of 0.5 M phenol. FeTPP (1 mM) in DMF + 0.1 M *n*-Bu_4NPF_6. a: cyclic voltammogram starting with Fe(II)TPP. b: Fe(I/0) catalytic wave. c: FOW analysis of the catalytic wave (E^0_{PQ} = −1.428 V vs SHE). d: variation of the observed rate constant with CO_2 concentration.

Scheme 2

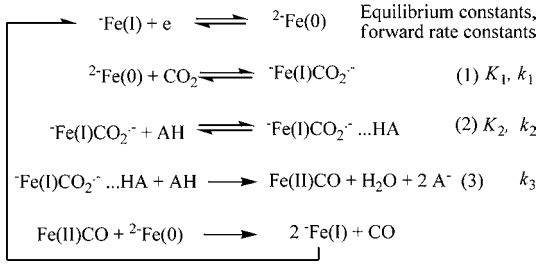

Table 2. Kinetic Constants

AH	pK[26]	K_1k_2 (M^{-2} s^{-1})	$K_1K_2k_3$ (M^{-3} s^{-1})	$K_1K_2k_3$ KIE
H_2O	31.5	–	10^2	–
TFE	24.0	–	8×10^4	1.8
PhOH	18.8	4×10^4	8×10^6	2.5
AcOH	13.3	6×10^5	1.2×10^8	1.5

intramolecular electron transfer process while the other one is preserved in CO. It follows that the reaction goes through the Fe^{I} asymmetrical adduct rather than the Fe^{II} symmetrical adduct. In the reverse reaction the precursor complex may also take two forms, corresponding to a Fe^{I} and a Fe^{II} mesomeric form: $^{-}$Fe(I)·$^{+}$C═O and Fe^{II}:C═O, respectively, giving rise to the two adducts shown at the bottom of Scheme 3, the reaction going through the Fe^{II} adduct rather than through the Fe^{I} adduct. The bond cleavage process may therefore be described as an intramolecular concerted dissociative electron transfer (CETBC) which may (CPETBC) or may not (stepwise process) be concerted with proton transfer as depicted in Scheme 3. We may now attempt to discriminate between the three pathways shown in Scheme 3 on the basis of the variations of the kinetic

Scheme 3

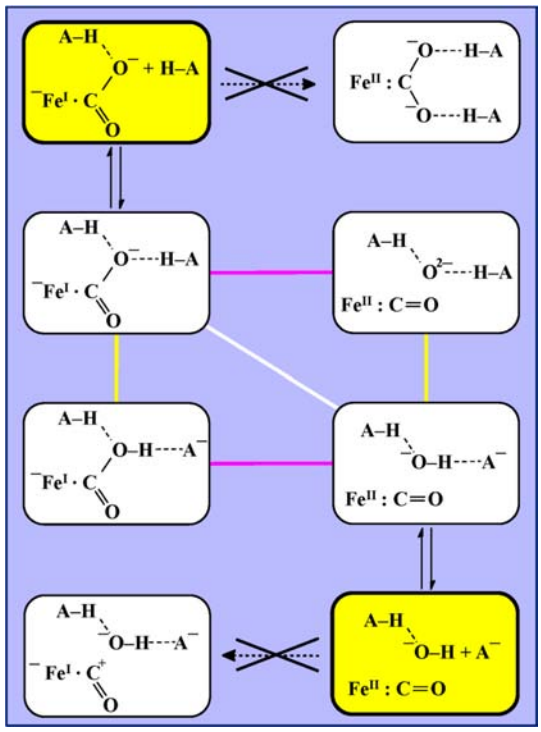

constant $K_1K_2k_3$ with the pK of the added acid (Table 2). A linear correlation between log $K_1K_2k_3$ and the pK is found, with a slope of −0.35 (Figure 7), which reflects the variation of log K_2k_3 with

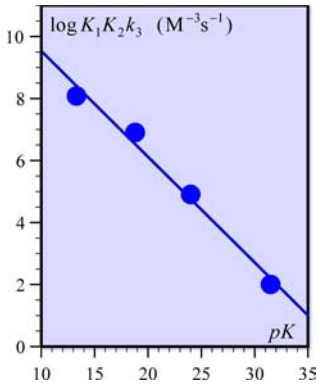

Figure 7. Variations of the kinetic constant $K_1K_2k_3$ with pK of the added acid.

the pK because K_1, the equilibrium constant for the formation of the initial adduct between the iron(0) porphyrin and CO_2, is expected to be independent of the pK.

In view of the lack of correlation between H-bonding ability and pK,[27] K_2 may also be considered as approximately constant in the series. The linear correlation in Figure 7, with its Brönsted slope of 0.35 may therefore be viewed as a Brönsted relation between log k_3 and the acid pK. This observation rules out a mechanism in which a reversible proton transfer (PT) would precede a CETBC rate-determining step in which case the Brönsted slope would be 1. If, conversely, in a PT + CETBC pathway, the initial proton transfer is not at equilibrium but is the rate-determining step, then, because the anion radical of CO_2 is a strong oxygen base, its protonation is expected to be independent of the

dx.doi.org/10.1021/ja4030148 | J. Am. Chem. Soc. 2013, 135, 9023−9031

acid pK, being close to the diffusion limit. Consequently, the stepwise PT + CETBC pathway can be ruled out. We may also dismiss the other stepwise pathway (CETBC + PT) in which, starting from the doubly H-bonded structure, bond cleavage would be rate the rate-determining step followed by a fast protonation. Indeed, this would involve the very unlikely formation of an intermediate in which the oxygen atom would bear two negative charges.

It thus appears that the only viable pathway involves as rate-determining step an electron transfer from the iron center concerted with proton transfer and C−O bond cleavage (CPETBC). The experimental value of 0.35, clearly below 0.5, is typical of reaction in which bond breaking and electron transfer are concerted,[28] thus validating further the description of the bond cleavage as an intramolecular dissociative electron transfer.

The concerted proton−electron transfer character of the CPETBC pathway is consistent with the H/D kinetic isotope effect found upon addition of hydrogenated and deuterated acids (Table 2). For each acid, $K_1K_2k_3$ has been measured using the FOW analysis within a concentration range suitable to get a reaction order of 2 in added acid ($k_{ap} = K_1K_2k_3[AH]^2$), i.e., from 0.1 to 1 M with CF_3CH_2OH, from 1 to 5 mM with acetic acid, and from 1 to 20 mM with phenol (Figure 8). The potential

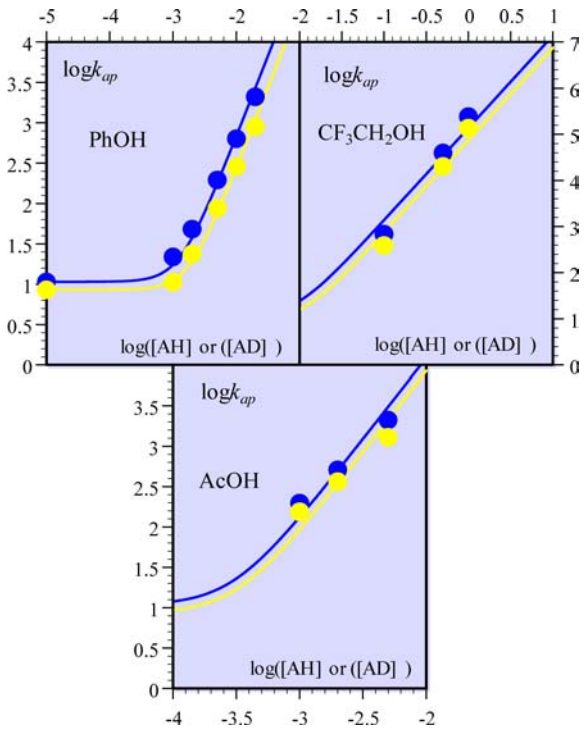

Figure 8. Variations of the apparent catalytic rate constant with the concentration of acids in the presence of hydrogenated acid (blue) or deuterated acid (yellow). Concentrations in M, k_{ap} in M^{-1} s^{-1}. Solid lines: fitting according to $k_{ap} = k_i + K_1K_2k_3[AH]^2$.

energy profiles for the rate-determining CPETBC step of the acid-boosted catalysis of the reduction of CO_2 to CO by iron(0)TPP are shown in Figure 9 by reference to the model developed for the CPETBC of a O−O bond in an organic peroxide containing an appended carboxylic acid function.[23] It is derived from two successive applications of the Born−Oppenheimer approximation. In the first, the transition state is obtained by intersection of the potential energy curves relative to the heavy atoms. The main component of the reaction coordinate is the

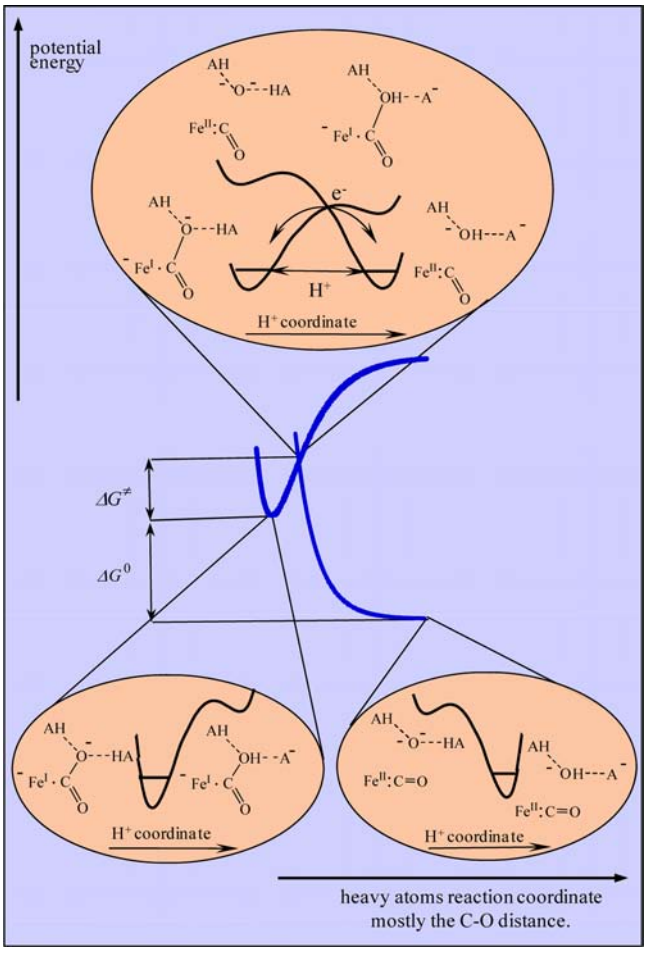

Figure 9. Potential energy profiles for the concerted proton−electron bond cleavage rate-determining step of the acid-boosted catalysis of the reduction of CO_2 to CO by iron(0)TPP.

C−O distance in the bond being broken. As a function of this distance, the reactant and product potential energy profiles may be represented by a Morse curve and a repulsive Morse curve (blue curves in Figure 9) as in the theory of dissociative electron transfer in which a bond is broken upon electron transfer with no interference of proton transfer.[29] The upper blowup insert shows the potential energy profiles vs proton coordinate resulting from the second application of the Born−Oppenheimer approximation, for the fixed geometry of the heavy atoms at the transition state. The two curves represent the variation of the potential energy with the proton coordinate of two diabatic electronic states, one for the reactants and the other for the products. Proton transfer is assumed to be adiabatic on each of these electronic states, leading to four local minima characterized by the geometries shown in the insert. Electron transfer takes place at the intersection between the two diabatic curves, while protons tunnel through the barrier they form. The activation free energy is thus obtained by the intersection of the two blue curves, leading to the same relationships as dissociative electron transfer with no interference of proton transfer.[29] Proton tunneling interferes with the pre-exponential factor and is the cause of a H/D kinetic isotope effect larger than 1.

EXPERIMENTAL SECTION

Chemicals. Dimethylformamide (Acros, >99.8%, extra dry over molecular sieves), the supporting electrolyte NBu_4PF_6 (Fluka, purriss.), *meso*-tetraphenylporphyrin iron(III) chloride (Aldrich), phenol

dx.doi.org/10.1021/ja4030148 | J. Am. Chem. Soc. 2013, 135, 9023−9031

(Alfa-Aesar), CF_3CH_2OH (Alfa-Aesar), AcOH (Prolabo), PhOD (Sigma-Aldrich), CD_3COOD (Sigma-Aldrich), CF_3CD_2OD (Euriso-Top), and D_2O (Euriso-Top) were used as received.

Methods and Instrumentation. *Cyclic Voltammetry.* The working electrode was a mercury drop hung to a 1 mm diameter gold disk. The counter-electrode was a platinum wire and the reference electrode an aqueous SCE electrode. All experiments were carried out under argon or carbon dioxide at 21 °C, the double-wall jacketed cell being thermostated by circulation of water. Cyclic voltammograms were obtained by use of a Metrohm AUTOLAB instrument. Ohmic drop was compensated using the positive feedback compensation implemented in the instrument. Each voltammogram is an average of at least three voltammograms recorded on different mercury drops.

Electrolysis. Electrolyses were performed using a Princeton Applied Research (PARSTAT 2273) potentiostat. The experiments were carried out in a two-compartment cell with a mercury pool as working electrode. The reference electrode was an aqueous SCE electrode and the counter-electrode a platinum wire in a bridge separated from the cathodic compartment by a glass frit, containing a 0.4 M $Et_4NCO_2CH_3$ + 0.1 M NBu_4PF_6 DMF solution. The electrolysis solution was purged with CO_2 during 20 min prior to electrolysis.

Particular care was exerted to minimize the ohmic drop between working and reference electrodes. This was performed as follows: the reference electrode was directly immersed in the solution (without separated bridge) and put progressively closer to the working electrode until sustained oscillations appeared. It was then moved slightly away until the remaining oscillations were compatible with the catalytic current. The appearance of oscillations in this cell configuration does not require positive feedback compensation as it does with microelectrodes. The potentiostat + positive feedback compensation device system is equivalent to a self-inductance.[29] Oscillations thus appear as soon as the resistance that is not compensated by the potentiostat comes close to zero as the reference electrode comes closer and closer to the working electrode surface.

Gas Detection. Gas chromatography analyses of gas evolved in the course of electrolysis were performed with a HP 6890 series equipped with a thermal conductivity detector (TCD). CO and H_2 production was quantitatively detected using a carbosieve S III 60−80 mesh column 2 m in length and 1/8 in. in diameter. Temperatures were held at 230 °C for the detector and 34 °C for the oven. The carrier gas was helium flowing at constant pressure with a flow of 20 mL/min. Injection was performed via a syringe (500 μL) previously purged with CO_2. The retention time of CO was 7 min. Calibration curves for H_2 and CO were determined separately by injecting known quantities of pure gas.

CONCLUDING REMARKS

Addition of Brönsted acids boosts the catalysis of CO_2 reduction to CO by electrogenerated iron(0)TPP. With examples of four acids, water, trifluoroethanol, phenol, and acetic acid, the exact boosting role of the acids was systematically interrogated. Because it avoids spurious side-phenomena, application of the foot-of-the wave strategy to cyclic voltammetric responses from the catalysis of CO_2 reduction to CO as a function of acid addition allowed the reaction orders for added acid to be derived. The systematic application of the FOW strategy to the derivation of reaction orders as exemplified here may serve as a model for numerous reactions where electron transfer breaking of a bond is assisted by proton transfer, as for example, within the scope of CO_2 reduction to CO, the catalytic reactions described in refs 14 and 30. Based on a large number of data where the concentration of acid and the amount of water were systematically varied, the mechanism of the catalytic process could be established and the main kinetic characteristics could be obtained. It appears that the rate-determining step is a reaction in which electron transfer from the central iron atom is concerted with proton transfer and breaking of one C−O bond along with an intramolecular CPETBC reaction. This is the second example where such a CPETBC reaction has been recognized and characterized as such. This reaction is thus relevant for the same kinetic model as that developed and applied to the electrochemical cleavage of an O−O bond. It is the first time that such a concerted proton−electron transfer-bond cleavage reaction has been unambiguously detected and characterized in the course of a catalytic process as the first example of most probably a very common event in molecular catalysis.

ASSOCIATED CONTENT

Supporting Information

Additional data. Analysis of the catalysis kinetics. This material is available free of charge via the Internet at http://pubs.acs.org.

AUTHOR INFORMATION

Corresponding Author

cyrille.costentin@univ-paris-diderot.fr; saveant@univ-paris-diderot.fr

Notes

The authors declare no competing financial interest.

ACKNOWLEDGMENTS

Partial financial support from the Agence Nationale de la Recherche (ANR 2010 BLAN 0808) is gratefully acknowledged.

REFERENCES

(1) (a) The standard potential of the $CO_2/CO_2^{\bullet-}$ couple has been estimated to be −1.97 V vs SHE in *N*,*N*′-dimethylformamide + 0.1 M Et_4NClO_4. The standard rate constant was 6×10^{-3} cm/s with a transfer coefficient of 0.4.[1b] (b) Lamy, E.; Nadjo, L.; Savéant, J.-M. *J. Electroanal. Chem.* **1977**, *78*, 403.

(2) Savéant, J.-M. *Chem. Rev.* **2008**, *108*, 2348.

(3) Benson, E. E.; Kubiak, C. P.; Sathrum, A. J.; Smieja, J. M. *Chem. Soc. Rev.* **2009**, *38*, 89.

(4) Rakowski Dubois, M.; Dubois, D. L. *Acc. Chem. Res.* **2009**, *42*, 1974.

(5) Bourrez, M.; Molton, F.; Chardon-Noblat, S.; Deronzier, A. *Angew. Chem., Int. Ed.* **2011**, *50*, 9903.

(6) Windle, D.; Perutz, R. N. *Coord. Chem. Rev.* **2012**, *256*, 2562.

(7) Costentin, C.; Robert, M.; Savéant, J.-M. *Chem. Soc. Rev.* **2013**, *42*, 2423.

(8) Smieja, J. M.; Sampson, M. D.; Grice, K. A.; Benson, E. E.; Froehlich, J. D.; Kubiak, C. P. *Inorg. Chem.* **2013**, *52*, 2484.

(9) Froehlich, J. D.; Kubiak, C. P. *Inorg. Chem.* **2012**, *51*, 3932.

(10) Fisher, B. J.; Eisenberg, R. *J. Am. Chem. Soc.* **1980**, *102*, 7361.

(11) Hawecker, J.; Lehn, J.-M.; Ziessel, R. *J. Chem. Soc. Chem. Commun.* **1984**, 328.

(12) Chen, Z.; Chen, D.; Weinberg, D. R.; Kang, P.; Concepcion, J. J.; Harrison, D. P.; Brookhart, M. S.; Meyer, T. J. *Chem. Commun.* **2011**, *47*, 12607.

(13) (a) Bhugun, I.; Lexa, D.; Savéant, J.-M. *J. Am. Chem. Soc.* **1994**, *116*, 5015. (b) Bhugun, I.; Lexa, D.; Savéant, J. M. *J. Am. Chem. Soc.* **1996**, *118*, 1769. (c) Bhugun, I.; Lexa, D.; Savéant, J.-M. *J. Phys. Chem.* **1996**, *100*, 19981.

(14) Wong, K.-Y.; Chung, W.-H.; Lau, C.-P. *J. Electroanal. Chem.* **1998**, *453*, 161.

(15) Bhugun, I.; Lexa, D.; Savéant, J.-M. *J. Am. Chem. Soc.* **1996**, *118*, 3982.

(16) (a) Costentin, C.; Drouet, S.; Robert, M.; Savéant, J.-M. *J. Am. Chem. Soc.* **2012**, *134*, 11235. (b) Costentin, C.; Drouet, S.; Robert, M.; Savéant, J.-M. *J. Am. Chem. Soc.* **2012**, *134*, 19949. (c) Costentin, C.; Drouet, S.; Robert, M.; Savéant, J.-M. *Science* **2012**, *338*, 90.

(17) (a) For recent overviews on proton-coupled electron transfers see refs 17b, c. (b) Hammes-Schiffer, S. *Chem. Rev.* **2010**, *110*, 6937. (c) Savéant, J.-M. *Energy Environ. Sci.* **2012**, *5*, 7718.

(18) Biczok, L.; Linschitz, H. *J. Phys. Chem.* **1995**, *99*, 1843.

(19) (a) Rhile, I. J.; Mayer, J. M. *J. Am. Chem. Soc.* **2004**, *126*, 12718. (b) Markle, T. F.; Mayer, J. M. *Angew. Chem., Int. Ed.* **2008**, *47*, 564.
(20) (a) Hammes-Schiffer, S. *Acc. Chem. Res.* **2009**, *42*, 1881. (b) Hammes-Schiffer, S. *Energy Environ. Sci.* **2012**, *5*, 7696.
(21) Song, N.; Stanbury, D. M. *Inorg. Chem.* **2008**, *47*, 11458.
(22) Weinberg, D. R.; Gagliardi, C. J; Hull, J. F.; Fecenko Murphy, C.; Kent, C. A.; Westlake, B. C.; Paul, A.; Ess, D. H.; McCafferty, D. G.; Meyer, T. J. *Chem. Rev.* **2012**, *112*, 4016.
(23) Costentin, C.; Hajj, V.; Robert, M.; Savéant, J.-M.; Tard, C. *Proc. Nat. Acad. Sci. U.S.A.* **2011**, *108*, 8559.
(24) (a) Savéant, J.-M.; Vianello, E. In *Advances in Polarography*; Longmuir, I. S., Ed.; Pergamon Press: London, 1960; pp 367−374. (b) Savéant, J.-M.; Su, K. B. *J. Electroanal. Chem.* **1984**, *171*, 341. (c) Savéant, J.-M. *Elements of Molecular and Biomolecular Electrochemistry*, Wiley-Interscience: New York, 2006; Chap. 2, pp 108−119.
(25) Scheer, H. *Chlorophylls and bacteriochlorophylls: Biochemistry, biophysics, function and applications*; Grimm, B.; Porra, R. J.; Rüdiger, W.; Sheer, H., Eds.; Springer: Dordrecht, The Netherlands, 2006; Chap. 1.
(26) Andrieux, C. P.; Gamby, J.; Hapiot, P.; Savéant, J.-M. *J. Am. Chem. Soc.* **2003**, *125*, 10119.
(27) Abraham, M. H.; Grellier, P. L.; Prior, D. V.; Morris, J. J.; Taylor, P. J. *J. Chem. Soc., Perkin Trans. 2* **1990**, 521.
(28) (a) Savéant, J.-M. *J. Am. Chem. Soc.* **1987**, *109*, 6788. (b) Reference 24c, chap. 3
(29) Reference 24c, chap. 1.
(30) (a) DuBois, D. L.; Miedaner, A.; Haltiwanger, R. C. *J. Am. Chem. Soc.* **1991**, *113*, 8753. (b) Bernatis, P. R.; Miedaner, A.; Haltiwanger, R. C.; DuBois, D. L. *Organometallics* **1994**, *13*, 4835.